ELSEVIER

Computers in Biology and Medicine 37 (2007) 1709–1718

Computers in Biology and Medicine

www.intl.elsevierhealth.com/journals/cobm

Bone drilling haptic interaction for orthopedic surgical simulator

Ming-Dar Tsai[a], Ming-Shium Hsieh[b,*], Chiung-Hsin Tsai[c]

[a]*Institute of Information and Computer Engineering, Chung Yuan Christian University, Chung Li 32023, Taiwan, ROC*
[b]*Department of Orthopaedics and Traumatology, Taipei Medical University Hospital, Taipei Medical University, 252, Wu Hsing Street,*

[c]*Department of Mechanical Engineering, Lunghwa University of Science and Technology, 300 Wan-shou Rd., Sec.1, Kueishan Taoyuan, Taiwan, ROC*

data) for arthroscopic or oral implant or nose surgery [16–18]. We also developed a volume based orthopedic simulator that extends voxel contents to represent bone boundary topology and geometry and thus to enable the closure check for the intersections of tool-swept surfaces with any bone. This simulator then recognizes new bones generated from the cut swept surfaces on the bone to enable various orthopedic surgical procedures such as to delete, reposition and fuse bones. The simulator also transforms prosthetic components or surgical tools such as drills into the representation of volume data to implement Boolean (e.g., subtraction) operations between the tools or prosthetic components with the bone. Surgeons can use this simulator to open, reposition and close a bone, or insert a prosthesis, or implement screws and plate on the virtual patient generated from the volume [19]. The simulation results have been used to assist verifications and diagnoses about spine [20–22], knee [23,24], hip [25] and maxillofacial [26,27] surgeries. Several simulation examples for screws and plate including hole drilling are introduced [25].

Several surgical simulation systems have already presented haptic functions to provide the tactical environment and thus to improve training effects. Most of these haptic responses involve deformable organs [28–32]. Some involve bone removal, such as burring and sawing operations. The bone burring simulations use a model assuming that the cutting force is proportional to the immersed depth of the bur into the bone or the tooth [33,34]. Meanwhile, the bone sawing simulation uses the model that describes bone chip removal loads on the oscillating saw teeth to represent cyclic sawing force [35]. Because interns should experience vibrating sawing force, such force prediction is useful for training. Bone drilling resembles bone sawing and thus requires a model that describes bone chip removal loads on the rotating drill chisel edge and cutting lips to represent the cyclic vibrating force. Such force computation model has been discussed in metal drilling [36–39].

This paper introduces haptic functions added to our reported orthopedic surgical simulator for simulating the bone drilling process. These functions represent haptic responses when using a virtual drill to touch or drill a bone. The system uses a 6D position-sensing haptic device to simulate the drill position and angle that are then used to calculate whether the virtual drill has immersed into any bone in the patient-specific volume. The geometric information about the bone immersing is then used to calculate the touch resistance against an uncut drill, and the drilling force for rendering the forces to the haptic device as well as the drilling torque for evaluating the work for bone drilling, drill bend and hand-piece oscillation. The rest of this paper is as follows. Section 2 introduces the system structure. Section 3 introduces the method of using the 6D haptic device input data to determine the drill position, angle, and linear and rotational speed. Section 4 introduces the touch resistance model that computes a force against the bone penetration from the drill not in the cutting status. Section 5 introduces the force and torque computation models that summate the loads on the rotating chisel and lips to obtain the cyclic drilling forces and torques. Section 6 demonstrates a simulation example of screw and plate surgery applying these haptic functions. Finally, discussion and future works are drawn in Section 7.

2. Volume based orthopedic surgery simulator

Fig. 1 shows the system architecture. The computer is a dual CPU P-IV 3.0 G with the graphics card of QUADRO4_980_XGL by NVIDIA Inc. The haptic device is a PHANToM Desktop by SensAble Inc. This device has been widely used and obtained high reliability [40]. The software is implemented in C + + (Visual C + + ver. 5.0) using the OpenGL libraries to render isosurfaces, and using the HDDIV libraries (by SensAble Inc.) to obtain the 6D haptic device data (representing the x, y, z coordinates and the angles about the x-, y- and z-axes of the haptic device, respectively) and to render this device (generating three translational forces along the x-, y- and z-axes, respectively).

The system provides menus and data bars to let users choose a volume to simulate, determine a simulation function to operate, choose a drill or a plate or a screw for screw and plate surgery. This volume is constituted by a set of CT or MRI slices. The data conversion process converts every original gray-level voxel in this volume as a voxel with six pairs of face flags and distance-levels that can dynamically represent the topology and geometry changes of bones around the voxel. A distance-level means a distance from the voxel center to the bone boundary (isosurface) and is determined from the gray-level threshold (representing the bone boundary) and the voxel value (gray-level). For a CT volume, the thresholds for cortical and cancellous bones are visually determined from the slices constituting the volume. For a MRI volume, the thresholds are determined by manually bordering on each slice. The isosurface reconstruction process based on the marching cubes algorithm reconstructs triangulated isosurfaces by the vertices determined from the thresholds and the distance-levels of the voxels. The rendering process renders the isosurfaces and the drill through the OpenGL libraries. Real-time re-rendering can be achieved when changing the perspective because of no isosurface reconstruction.

The haptic device input process catches the 6D input information of the haptic device in a specified haptic sample frequency (set herein 1000 Hz) to simulate the position and angle of a tool that can be a saw or an osteotome. The saw or

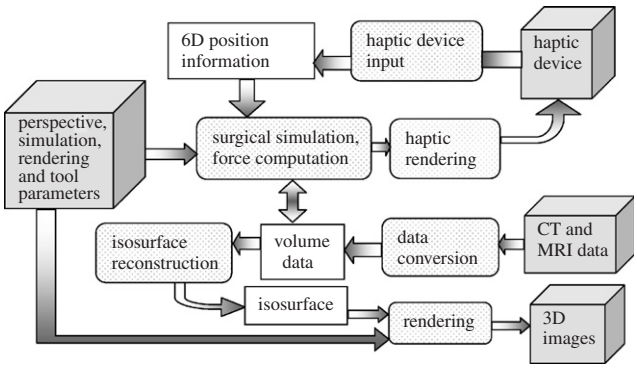

Fig. 1. System architecture.

osteotome edge from two tool positions and angles determines an edge swept surface that is used to simulate bone cutting. If one or more swept surfaces form a closed surface inside a bone, seed filling changes the closed voxels as a new bone or null to simulate a bone separation or removal [19]. Conversely, the seed in a bone structure can be used to fill voxels until reaching the boundary of another bone to simulate a postoperative bone fusion and regeneration. A bone reposition writes the contents of all solid voxels into the ones in new positions. A Boolean operation between a bone with a solid simulates a subtraction between a bone with a drill or an insertion (addition) of a prosthetic component or a bone graft into a bone [19]. The drill solid is determined by the position, angle and size of the chosen drill.

These 6D inputs of successive haptic intervals are used to calculate linear and rotational drill speeds. The force computation process then uses the drill position and speed to compute the touch resistance or the drilling force and torque. The touch resistance and drilling force are used for haptic rendering. During the drilling process simulation, the geometric changes of bones are not computed (i.e., no isosurface reconstruction) until the process is finished. Therefore, the real-time visual refresh requirement (30 Hz) can be achieved for rendering bones and the drill at the new drill position. Meanwhile, the system summates the forces from sample points on a drill to calculate the touch resistance or the drilling force and torque. Therefore, the sample point interval determines the computation accuracy and speed. The small interval leads high accuracy but lower the speed. Therefore, the interval is set as achieving the highest accuracy but can satisfy the requirement of 1000 Hz haptic responses even under the largest bone applied drill. Under such haptic responses, every revolution in general rotation numbers (500–1500 rpm) can traverse 40–120 haptic intervals that are enough to represent the cyclic drilling forces and torques.

3. Tool position and speed computation

The pen-like haptic device attached with a drill (as shown Fig. 2(A)) is used to simulate a real drill attached hand-piece (as illustrated in Fig. 2(B)). The drill axis is set as the q-axis of the drill coordinate system. The q-axis also matches the haptic pen direction, the z-axis of the haptic device coordinate system as illustrated in Fig. 2(C). The s-axis and t-axis are the other two primary axes of the drill coordinate system, meaning that the st-plane is parallel to the xy-plane and rotates as the drill rotates. The difference of the two vectors q and q' (the drill axis of the previous instant) becomes the rotation of the drill axis and the difference of the device positions P and P' becomes the drill translation. The rotation and translation dividing the haptic sample frequency determine the linear v and rotational ω velocities at P. The component of v along the drill axis direction (or q-axis) is defined as the feed speed, fq. The position and the velocities at P are then used to calculate the position and the linear velocity at every point of the drill. For example, the velocity at the drill origin C is equal to $v - \omega \times l$. l denotes the length from C to P.

The above haptic device coordinate (in real size) can be transformed into the volume coordinate (in voxel size) through the following concatenating transformations:

$$\begin{bmatrix} X \\ Y \\ Z \end{bmatrix} = S_{XZ} S_Y T R \begin{bmatrix} x \\ y \\ z \end{bmatrix}.$$

The scaling S_{XZ} corresponds to the inverse of the pixel width in the slices and is uniform for all tomographic slices that constitute the volume. The pixel width is obtained from FOV (field of view) dividing the voxel number in the slice wide. The scaling S_Y equals the inverse of the slice thickness. The translation T means the distance from the haptic device origin to the volume coordinate system origin. The rotation R corresponds to the angle between the volume and the haptic device coordinate systems and is constituted by three primary haptic device (x-, y- and z-axes) axes represented in the volume coordinate. Similarly, the volume coordinate can be transformed into the haptic device coordinate through the inversions of the above transformations.

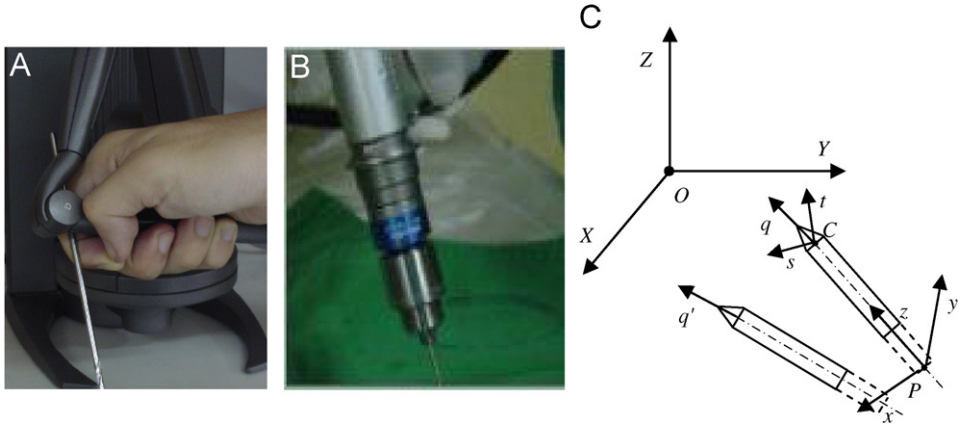

Fig. 2. Position and angle calculation for the virtual drill: (A) Haptic device for simulating a drill attached hand-piece; (B) A real drill attached hand-piece and (C) Drill position and angle determination using 6D data of haptic origin. P, C, O: origins of haptic device, drill coordinate system and volume coordinate system.

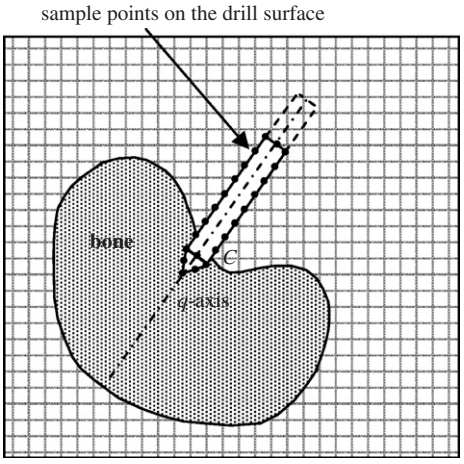

Fig. 3. Touch resistance computation.

4. Touch resistance computation

The penalty method is usually used to compute a force for preventing object penetration. This force is set as proportional to the penetrated depth. Therefore, object intersection computation is required to detect whether any object is penetrated by another object and then the penetrated depth from the object surface is computed to determine the penalty force [41]. We herein propose a method that does not implement the time-consuming object intersection and the penetrated depth computation but just detect how many sample points on the drill surface have immersed into bone voxels (with the gray-level values larger than the bone thresholds) for fast computation. More immersed points indicate the deeper penetrated depth; then a larger touch resistance is assigned.

The method first transforms the device coordinate of every preset sample point on the drill surface (as shown in Fig. 3) into the volume coordinate using the transformation equation described in Section 3. The three components of every transformed volume coordinate are rounded off to determine which voxel this sample point is located in. The sample point is inside a bone voxel and the drill is considered as already immersed into the bone at this point. The touch resistance is set proportional to the number of sample points inside bone voxels, because more immersed sample points represent the deeper the drill has penetrated the bone surface. The touch resistance direction is set as reversing the drill moving direction to oppose against the drill continuously moving into bones and pushes back the drill to the bone surface. From the drill end to 10 cm above at one voxel-width interval, the system rounds a circle on the drill surface to set sample points in one voxel-width interval. Therefore, totally about 2000 sample points are processed for a 5.4 mm drill (the largest drill used in the system).

5. Drilling force and torque computation

This system calculates the load on the cutting lips and chisel edge to obtain the drilling force as the method described in the machining theorem [36–38]. However, not as drilling by machines in which the feed direction can be precisely guided along the drill axis, the drill-attached hand-piece is not easily fed exactly along the drill axis direction. Therefore, our model also considers the effect of such manual feed, i.e., the sideways feed resistance and the feed change caused by the drill inclination from the drill axis direction. In our model, the cutting lips and the chisel edge are divided into small surface elements and the load acting on each element is computed and summated into the drilling force. A surface element (represented by a sample point) is judged as cutting the bone if this sample point locates inside any bone voxel (as the element of A or B illustrated in Fig. 4). That means the sample point is first transformed into the volume coordinate to check if it is in any bone voxel. If it is, the surface element is in drilling. The system then calculates the load for removing the bone chip on the element. Because sample points on the cutting lips and the chisel edge are in 0.1 mm interval, totally about 500 sample points should be processed for a large 5.4 mm drill.

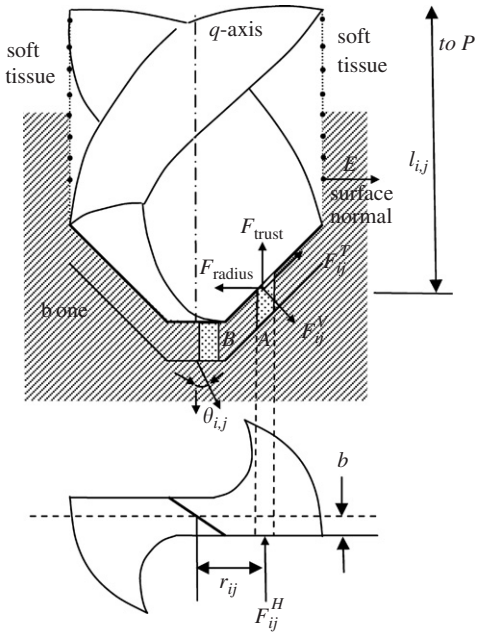

Fig. 4. Drilling force and torque computation.

5.1. Drilling force computation

The area of a cutting lip element (as A in Fig. 4) is calculated as $\mathrm{d}w \times f/n$. $\mathrm{d}w$ is the thickness of the equally divided surface elements. n is the number of the cutting lips. f is equal to $(fq - r_{i,j} \times \omega)/\mathrm{pps}$ (the drill rotation number per second). i denotes the ith cutting lip, and j denotes the jth divided surface element. $r_{i,j}$ is the distance of the element to the q-axis. $r_{i,j} \times \omega$ represents the effects of the feed change caused by the drill rotation. The load acting on the surface element is represented as the following three components (shown in Fig. 4):

$$F_{i,j}^H = \Delta K_H \cdot \mathrm{d}w \cdot f/n, \quad F_{i,j}^T = \Delta K_T \cdot \mathrm{d}w \cdot f/n,$$
$$F_{i,j}^V = \Delta K_V \cdot \mathrm{d}w \cdot f/n.$$

Δ is 1 if this element is inside a bone voxel (i.e., in drilling), otherwise it is 0. The above load components are then transformed and summated into the forces in tangential, trust (i.e., axial) and radial directions (Fig. 4). Therefore, the tangential (F_{tang}), trust (F_{trust}) and radial (F_{radius}) forces contributed by the cutting lip elements can be calculated by the following equations:

$$F_{\text{tang}} = \sum_{i,j} (F^H_{i,j}),$$

$$F_{\text{trust}} = \sum_{i,j} \left(\cos(\theta_{i,j}) \cdot F^T_{i,j} + \frac{\sqrt{(r^2_{i,j} - b^2)}}{r_{i,j}} \sin(\theta_{i,j}) \cdot F^V_{i,j} \right),$$

$$F_{\text{radius}} = \sum_{i,j} \left(\frac{\sqrt{(r^2_{i,j} - b^2)}}{r_{i,j}} \sin(\theta_{i,j}) \cdot F^T_{i,j} - \cos(\theta_{i,j}) \cdot F^V_{i,j} \right).$$

The area of a chisel edge element (as B in Fig. 4) is calculated as $\mathrm{d}w \times f$. Because the radius of the chisel edge element to the drill axis is small, the effect of the feed rate change caused by the drill rotation is small to be neglected. Therefore, f is herein set as fq/pps. Then, the trust force on this element is calculated as $F^C_j = \Delta K_C \cdot dw \cdot f$. j denotes the jth divided surface element. Δ is 1 if this element is inside a bone voxel, otherwise it is 0. By summing up the trust forces of all chisel edge elements, the trust force contributed by the chisel edge is calculated as $F_{\text{trust}} = \sum_j (F^C_j)$.

F_x, F_y and F_z are the forces rendered to the x-, y- and z-directions, the three primary axes (as illustrated in Fig. 3) of the haptic device, and therefore are the ones the user feels. F_z is equal to F_{trust} because the trust force acts along the q-axis of the drill, i.e., the z-axis of the haptic device. F_x and F_y are determined from F_{tang} and F_{radius} using the following equations:

$$F_x = \cos\alpha F_{\text{radius}} - \sin\alpha F_{\text{tang}},$$
$$F_y = \sin\alpha F_{\text{radius}} + \cos\alpha F_{\text{tang}}.$$

α represents the angle of the st-plane regarding the xy-plane. Because the st-plane (the drill) rotates, this changing α brings the cyclic F_x and F_y. Meanwhile, the force coefficients K_C, K_H, K_V and K_T actually depend on many variables such as the drill rake angle, point angle, helix angle, cutting velocity and feed rate, the bone density, and the radius from the drill axis to the element etc. Herein, K_H, K_V and K_T are set as linear functions of the radius from the surface element to the q-axis. Other variables regarding the drill geometry, bone types (cancellous or cortical) are determined empirically corresponding to the types of drills and bones.

5.2. Drilling torque computation

F_{tang} and F_{radius} from the cutting lip elements generate the torques T_{tang} and T_{radius}, simultaneously. T_{tang} works against the drill rotation and thus lets the hand-piece do the work for the drilling. T_{radius} bends the drill and thus brings a danger of drill breakage. T_{tang} and T_{radius} are calculated by the following equations:

$$T_{\text{tang}} = \sum_{i,j} (r_{i,j} \cdot F^H_{i,j}),$$

$$T_{\text{radius}} = \sum_{i,j} \left(l_{i,j} \cdot \left(\frac{\sqrt{(r^2_{i,j} - b^2)}}{r_{i,j}} \sin(\theta_{i,j}) \cdot F^T_{i,j} - \cos(\theta_{i,j}) \cdot F^V_{i,j} \right) \right).$$

$l_{i,j}$ denotes the distance from each element to the haptic point (the rotational center for this bending). F_{trust} from the cutting lip elements also generates the torque T_{trust} to let the machine oscillate around the q-axis. T_{trust} from the chisel edge can be neglected because of the small radius from the chisel edge to the q-axis. Therefore, T_{trust} is calculated as

$$T_{\text{trust}} = \sum_{i,j} \left(r_{i,j} \cdot \left(\cos(\theta_{i,j}) \cdot F^T_{i,j} + \frac{\sqrt{(r^2_{i,j} - b^2)}}{r_{i,j}} \sin(\theta_{i,j}) \cdot F^V_{i,j} \right) \right).$$

The PHANToM Desktop used in this system cannot output torques. However, the system represents T_{trust} as a cyclic force adding to F_{trust} that acts along the q-axis, because T_{trust} gives the user a feeling of oscillating around the q-axis. Meanwhile, F_{radius} is proportional to T_{radius} (in a ratio of $l_{i,j}$) and thus gives the user a similar sense as T_{radius}. Moreover, the user may make no sense about T_{tang} because it works against the drill rotation. Therefore, the system does not represent T_{tang} and T_{radius}.

5.3. Resistance against drilling sideways

The feed speed fq is the component of the drill velocity v along the feeding direction (as the q-axis shown in Fig. 4). However, the velocity component perpendicular to the q-axis (i.e., on the st-plane) brings a resistance to prevent the drill moving sideways (inclining to any direction on the st-plane) and thus to lead the drill moving along the q-axis direction. The system calculates this resistance as the following procedures. First, sample points (spaced in one voxel interval) on the drill surface except on the chisel edge and cutting lips are checked for any bone voxel inside. If a point (as E in Fig. 4) is in a bone voxel and the dot product of the surface normal at this point with fs (the velocity component on the st-plane) is positive, a force proportional to the dot product occurs at this point. Therefore, the resistance that prevents the drill to move sideways is summated from the forces acting on the sample points.

6. Case study

Any series of CT slices following the DICOM (Digital Imaging and Communications in Medicine) protocol can be the

source data of our system. In the following, a patient with a typical open reduction and screw and plate surgery for trochanter fracture treated at the Orthopedic Department of Taipei Medical University Hospital in July 2001 was used to demonstrate the results implemented by our system. This 83-year-old man suffered from severe right hip pain with disability of right low leg. CT was performed in 95 transverse sections with 1 mm intervals at the hip (acetabulum, head, neck and trochanters) and 10 mm intervals in the stem and pelvis. Linear interpolations were implemented to obtain a volume with constant (1 mm) intervals.

Fig. 5(A) shows a 3D image that reveals a compression at the right trochanter by the femur neck. This compression results in a fracture passing from the lesser trochanter to the greater trochanter and a protrusion at the lesser trochanter. Fig. 5(B) shows the simulation results from the open-reduction surgery for the trochanter fracture and compression in which the stem was repositioned and the neck was lengthened to reduce the angle deviation. The system used our reported feature recognition and analysis methods that recognized the structures of trochanters and femur stem, analyzed the position, angle and size to determine the repositioned distance of the stem [25]. Therefore the angles of the femur stem and neck axes for the left and right hips became the same after the open reduction. As shown in Fig. 5(A), the user can choose any icon at the left top of the system window to open a dialog interface for choosing a patient, a perspective, simulation functions, rendering conditions, a tool, etc. For example, the user can choose a drill such as type, size and rotation number through the tool icon, then the dialog interface as illustrated in Fig. 5(B). The workspace of the haptic device automatically changes according to the perspective. The user can also modify this workspace by the device dialog interface slide bar to obtain an optimal workspace.

After the reduction, the screw and plate surgery was used to fix the femur stem onto the neck. For this screw and plate surgery, the user moved the chosen drill to the right hip but touched the hip as illustrated in Fig. 5(C). The system calculated the bone resistance to prevent the drill moving into the bone more and changed the drill color as light blue to reveal the touch. Because of this touch resistance, the user can only move the drill along the bone surface rather to penetrate the bone. One sample point corresponds to 0.1 N touch resistance force and the total resistance in the simulation was in 0.1–0.5 N, which is enough to notice the user has already touched bones. The user then drilled out four holes for inserting the screws as illustrated in Figs. 5(D)–(F). The system changed the drill color as red to reveal it was in drilling (as shown in Fig. 5(D)). Fig. 5(G) shows the screw and plate surgery has been implemented after the drilling. The reported feature recognition and analysis methods also analyzed the position, angle and size of the recognized femur stem and trochanters to determine the drilling positions and size, and then the positions and sizes of the screws and plate [25]. Therefore, the positions and sizes of the drill, screws and plate can correspond to the positions, angles and sizes of the femur stem and trochanters.

Fig. 6 illustrates F_x, F_y, F_z, T_{trust}, T_{tang} and T_{radius} from the beginning to the end in the first hole breakthrough (at the greater trochanter). The user tempted to keep the same feed speed along the drill axis direction and the rotational speed was set as the same during the drilling process. F_x, F_y and F_z were output to the haptic device and felt by the user. T_{trust}, T_{tang} and T_{radius} were the trust torque, tangential torque and radial torque that oscillated the hand-piece, opposed against the drill rotation and bended the drill, respectively. Because the rotating axes that T_{radius} and T_{trust} brought were changing, no direction but only the absolute values of T_{radius} and T_{trust} were demonstrated in Figs. 6(E) and (F), respectively. Seven stages can be observed from the drilling process: stages of drilling cortical bone (B and F), stage of drilling cancellous bone (D) and transitional stages (A, C, E and G).

T_{tang} and F_{trust} (F_z) were large at the cortical bone drilling stages (B and F) because both the cutting lips and the chisel edge were fully immersed in the hard cortical bones to drill, and T_{tang} and F_{trust} from the lip and edge elements all contributed the same direction to summate large values. At the bone drilling stages (B, D and F), T_{trust}, T_{radius}, F_{radius} and F_{tang} generated by the divided lip or edge elements cancel the ones generated by the symmetric elements; therefore, the summations and then the transformations F_x and F_y became small. However, T_{trust}, T_{radius}, F_x and F_y were large at the transitional stages because the symmetric elements of the cutting lips or edges may not be both in drilling or drilling the same type of (cortical or cancellous) bone to cancel T_{trust}, T_{radius}, F_x and F_y generated by the symmetric elements. T_{trust}, T_{radius}, F_x and F_y were especially large and all the forces and torques vibrate violently at the beginning stage (A). The reason can be considered to be that the large bone surface curvature led to the abrupt change in drilling geometry or let one cutting lip be not in drilling when the other lip was fully in drilling.

The calculated forces at the hole breakthrough resemble the tactile feeling from the real bone drilling. The calculated trust force profile shown in Fig. 6(A) also much resembles the drilling force profile measured from the real bone drilling [9]. These show the effectiveness of the drilling force and torque model.

7. Discussion and future woks

Surgical simulation systems allow surgeons to experience surgical procedures, and haptic interfaces enable perception and delicate tactile sensations required in surgery. The drilling process of orthopedic surgery is tough such that the violent vibration at the beginning of the drilling may bend the drill to break or let the user difficultly grasp the hand-piece. Such drilling haptic functions implemented in surgical simulations are important and have not yet developed. This study added haptic functions for drilling to an orthopedic surgical simulator so that not only geometric changes but also a tactile feeling of bone drilling can be provided for the simulation of screw and plate surgery. The combination of these haptic functions into the orthopedic surgical simulator that has been developed for visual verification, diagnoses and surgical planning provides a use of training interns and students with both tactile and visual interactions.

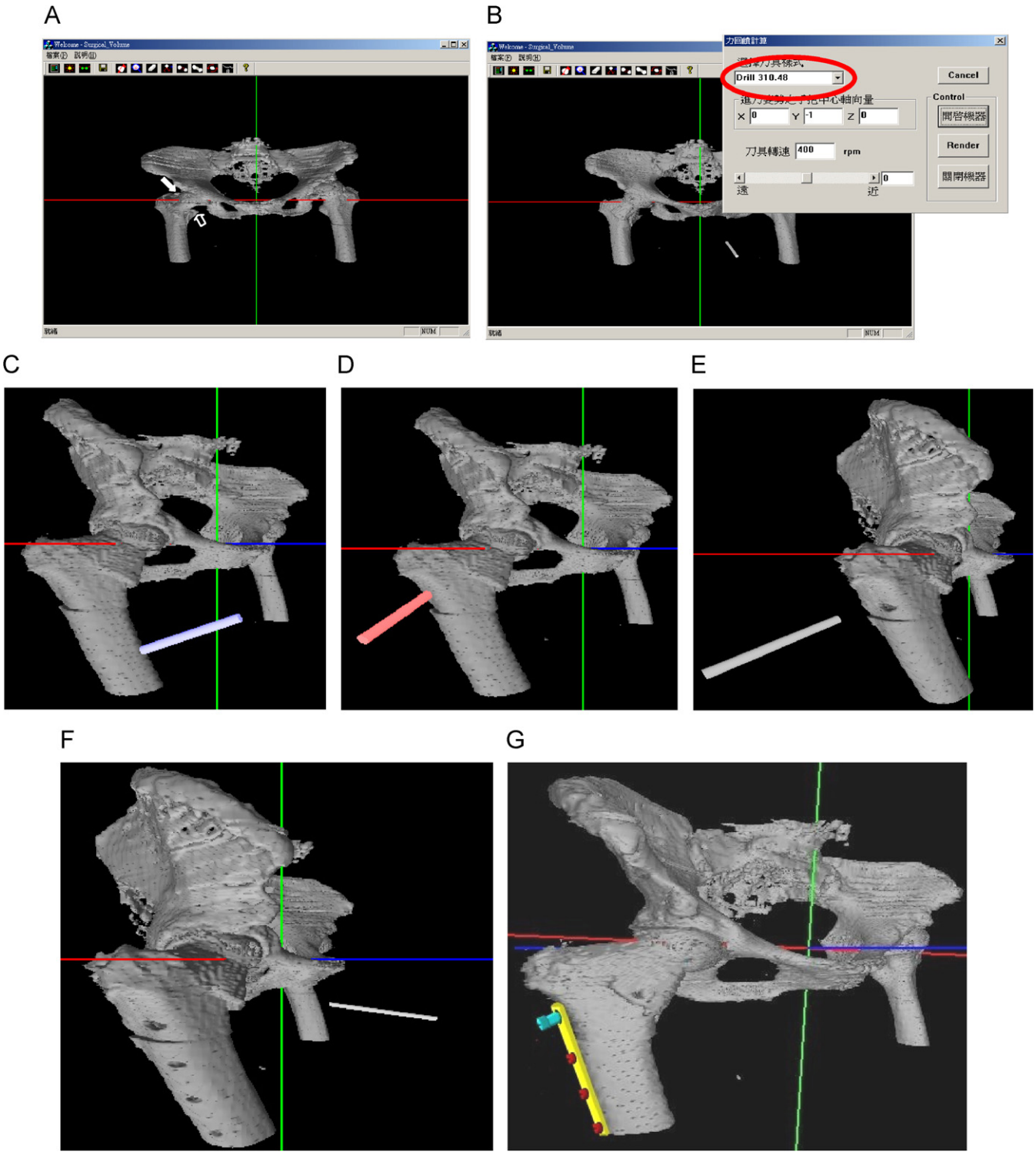

Fig. 5. Surgical simulations with haptic environment. (A) 3D reconstruction of bone surface before surgery. Frontal view. Solid arrow: fractured and angle-deviated right femur neck. Hollow arrow: protruded-out lesser trochanter. (B) 3D reconstruction of bone surface after correcting the trochanter fracture. Frontal view. Through each icon, one dialog interface can be opened. The red ellipse shows the chosen drill in the interface dialog. (C) The drill (light blue) has touched the bone with a resistance against the drill moving into the bone. Oblique view. (D) The drill (light red) is drilling the bone with cyclic forces and torques against the drilling. (E) Drilled hole has been shown. Oblique view. (F) All four drilled holes have been shown. Oblique view. Screws (red and blue) and plate (yellow): fixing the repositioned stem and neck. Oblique view.

Drilling theorems have been developed in machining field for many years and obtain confidences in their force computation models. Bone drilling resembles the metal drilling, therefore we adopted their models that calculate and then sum up the loads on divided surface elements on the cutting lips and chisel edge to obtain the tangential torque, and the trust, tangential

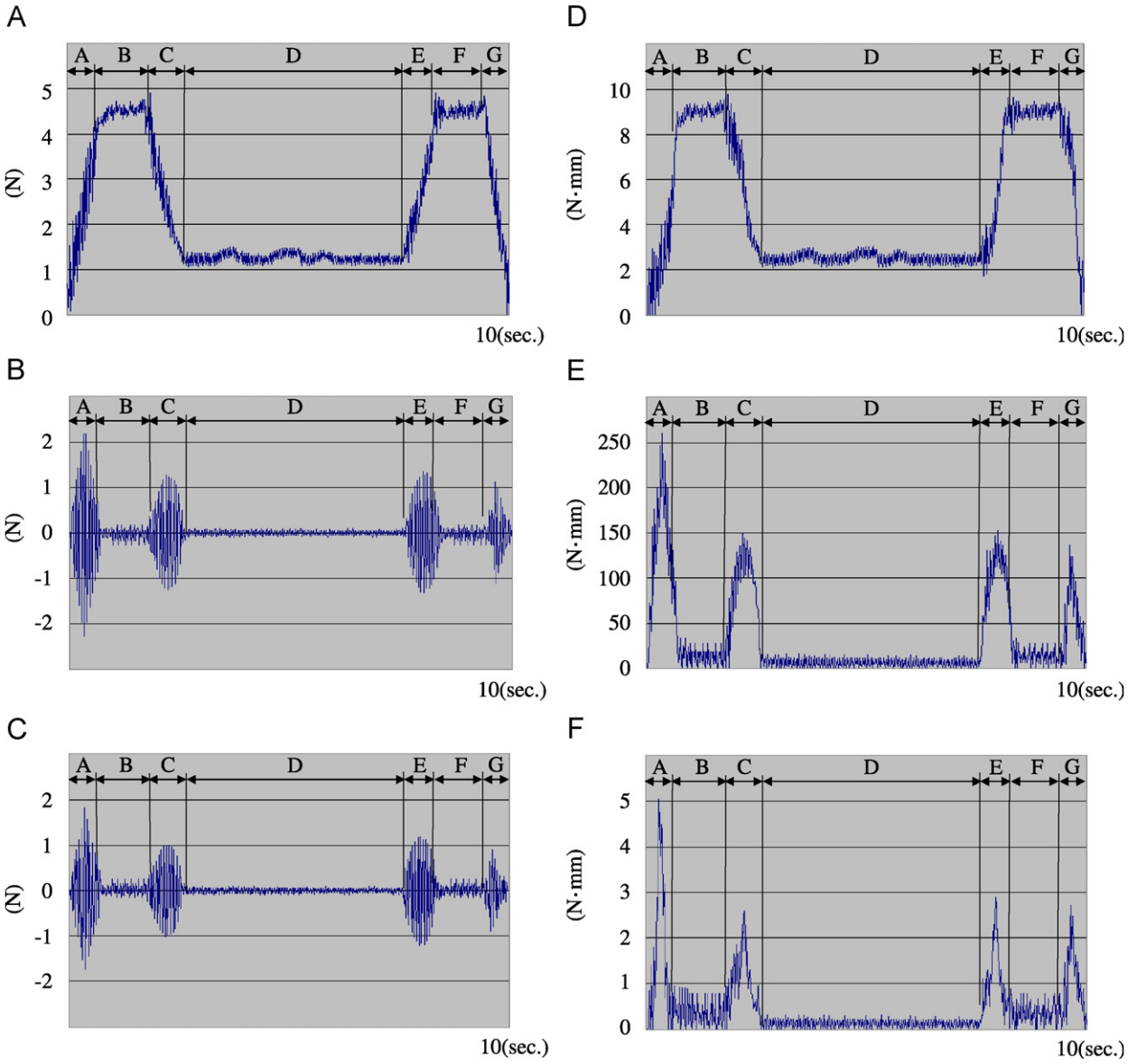

Fig. 6. Drilling forces and torques in a hole breakthrough on the greater trochanter. A stage: the beginning of the drilling, B and F stages: cortical bone drilling, D stage: cancellous bone drilling, C and E stages: transition between cortical and cancellous bone drilling, G stage: the ending of the drilling, N: force unit (Newton), N mm: torque unit. (A) Force along the z-axis of the haptic device. This axis is also the drill axis. (B) Force along the x-axis of the haptic device. This axis is also the haptic device axis. (C) Force along the y-axis of the haptic device. (D) Tangential torque. (E) Radial torque. (F) Trust torque.

and radial forces. These forces are then calculated as the forces that the user feels. We also extended the model to compute the tangential torque as the work for the drilling, and radial and trust torques for evaluating the drill bend and the hand-piece oscillation. Our prototype system manipulates the volume data of any specific patient to simulate the bone geometry changes during orthopedic surgery and bases on the manipulated bone geometry data together with the force and torque computation model to simulate the haptic responses in drilling the patient.

Although the simulated forces provide the tactile feeling that resembles the real drilling, the force coefficients in our models are simplified to neglect the effects of the drill rake angle, point angle, helix angle, cutting velocity and feed rate but only to consider the effect of bone (cortical and cancellous) types. To achieve higher predicted accuracy, these coefficients should be studied to vary according to the given specification (including age, sex, race, bone density and so forth) under statistically meaningful number of cases.

Another haptic response, the touch resistance, provides a touch feeling and a force to prevent the bone penetration when handling a non-rotating drill. This touch resistance computation model does not implement the time-consuming object intersection and penetrated depth computation. Therefore, this model can provide a real-time calculation by detecting whether the drill has already immersed into bone voxels and give a resistance as larger as deeper (more sample points) that the drill has immersed into. This force acts along the drill moving direction, and therefore, can push back the drill onto the bone

surfaces. The sample point interval herein is set as one voxel width to ensure no bone voxels are in-between any two sample points. Moreover, because the drill is usually moved under 10 cm/s (0.1 mm per haptic interval) in the non-drilling state, the haptic interval is much smaller than the sample point interval to give the user a real-time touch response when the drill begins immersing bone voxels. However, the sample point method leads to an aliasing problem, meaning that the number of immersed sample points may increase several immersed points at one time. Thus, the resulting touch resistance may not change smoothly. The resistance is not large, therefore will not give so uncomfortable haptic feeling.

Although a set of CT or MRI slices as the hip example provides voxels in 1 mm resolution level, the use of distance-level (256 levels in a voxel) determines the triangulated isosurface vertices in a sub-voxel level accuracy and provides fine 3D images by rendering the triangulated isosurfaces. Different human parts that are smaller than the hip possess smaller FOV (representing the size of each slice); therefore, finer resolution and then better 3D images can be expected. However, finer resolution lowers accuracy of the force and torque computation. Currently, the sample point interval for calculating the drilling forces and torques is set as a constant of 0.1 mm to achieve the haptic real-time. The sample point resolution equals 10 times the voxel resolution in the hip case. The same sample point resolution for a case with smaller FOV results in fewer sample points inside a voxel; thus, the resulting accuracy for drilling forces and torque computation becomes lower.

Meanwhile, the haptic interactions about the drilling force are usually felt stable. The reasons can be considered as follows. First, the haptic sample frequency (1000 Hz) by the PHANToM Desktop is far above the drill rotation frequency (about 1000 rpm) to not violate the Nyquist criteria and thus correctly simulate the rotation of the drilling force. The exerting force and the workspace ranges of the PHANToM Desktop are affordable for interactions between the user and the haptic interface. Second, the force computation can be real-time to provide stable simulations because our system just checks if sample points on the drill immersing into bone voxels rather uses time-consuming object intersection and penetrated depth computation to calculate the drilling force. Third, the touch resistance can notify the user that the drill is already on the bone to prevent a large feed during the beginning of drilling. Therefore, suddenly increased impedance that usually causes the instability in the haptic interactions can be usually avoided [42].

The prototype system provides a more economic, safe and convenient bone drilling training platform than by using synthetic bones or sectioned frozen bones or drilling on real patients. However, the validation of the prototype system should be evaluated by a number of experienced surgeons to compare the realism, precision, ease of use and help to surgery between using the simulation system and the traditional methods of using synthetic bones, sectioned frozen bones and real patients. This validation evaluation is our future work. Meanwhile, the haptic functions of the proposed system for extending are realizing a haptic device affordable to output the drilling torque and equipping the system with the second haptic device to simulate any guiding tool. Then, guided drilling that is also widely used in orthopedic surgery can be simulated using the proposed drilling force and torque model. The haptic functions for simulating other orthopedic surgery tools such as reaming and tapping bones as well as cutting, deforming and suturing soft tissues should also be our future works.

8. Summary

Successful execution of bone drilling requires high-level dexterity and experience because the drilling resistance is large and vibrates violently to difficultly grasp the hand-piece or even to break the slender drill. Therefore, combination of the drilling haptic functions into the orthopedic surgical simulator for training is important and has not yet developed until now. The proposed system manipulates the volume data of any specific patient to simulate the changes of bone geometry during orthopedic surgery and then uses the force and torque computation model to simulate the haptic responses in the drilling process based on the manipulated volume data.

Our force and torque computation model calculates and then sums up the loads on divided cutting lips and chisel edge elements to obtain forces and torques along the trust, tangential and radial directions. These forces are used to render the haptic device that provides the user tactile feeling. The calculated torques are used to evaluate the required work for drilling, the drill bend and the hand-piece oscillation during the drilling process.

A simulation example of screw and plate surgery demonstrates changes of bone geometry for several procedures and the calculated torques and forces during the drilling process of a hole breakthrough on the trochanter. The simulated forces and torques resemble the ones in real drilling and thus show the effectiveness of the drilling force and torque computation model.

Acknowledgment

This study was partially sponsored by the National Science Council (NSC), Taiwan/ROC; Grant nos. NSC-94-2213-E-033-028, NSC-95-2213-E-033-065.

References

[1] M.A. Karunakar, K.A. Egol, R. Peindl, M.E. Harrow, M.J. Bosse, J.F. Kellam, Split depression tibial plateau fractures: a biomechanical study, J. Orthop. Trauma 16 (2002) 172–177.
[2] M.E. Müller, M. Allgower, R. Schneider, H. Willeneger, Manual of Internal Fixation, third ed., Springer, Berlin, Heidelberg, New York, 1991 pp. 598–600.
[3] A.D. Steffee, R.S. Biscup, D.J. Sitkowski, Segmental spine plates with pedicle screw fixation, Clin. Orthop. Rel. Res. 203 (1986) 45–53.
[4] G.D. Carlson, J.J. Abitbol, D.R. Anderson, et al., Screw fixation in the human sacrum, Spine 17 (1992) S196–S203.
[5] A. Marti, C. Fankhauser, A. Frenk, J. Cordey, B. Gasser, Biomechanical evaluation of the less invasive stabilization system for the internal fixation of distal femur fractures, J. Orthop. Trauma 15 (2001) 482–487.
[6] M.J. Prayson, D.K. Datta, M.P. Marshall, Mechanical comparison of endosteal substitution and lateral plate fixation in supracondylar fractures of the femur, J. Orthop. Trauma 15 (2001) 96–100.

[7] K.C. Booth, T.K. Donaldson, Q.G. Dai, Femoral neck fracture fixation: a biomechanical study of two cannulated screw placement techniques, Orthopedics 21 (1998) 1173–1176.
[8] R.L. Uhl, The biomechanics of screws, Orthop. Rev. 18 (1989) 1302–1307.
[9] F.R. Ong, K. Bouazza-Marouf, The detection of drill bit break-through for the enhancement of safety in mechatronic assisted orthopaedic drilling, Mechatronics 9 (1999) 565–588.
[10] W.Y. Lee, C.L. Shih, Control and breakthrough detection of a three-axis robotic bone drilling, Mechatronics 16 (2006) 73–84.
[11] R.F. McLain, E. Sparling, D.R. Benson, Early failure of short-segment pedicle instrumentation for thoracolumbar fractures, J. Bone Joint Surg. 75A (1993) 162–167.
[12] W.L. Foley, D.E. Frost, M.R. Tucker, The effect of repetitive screw hole use on the retentive strength of pretapped and self-tapped screws, J. Oral Maxillofac. Surg. 48 (1990) 264–267.
[13] C.T. Vangsness, D.R. Carter, V.H. Frankel, In vitro evaluation of the loosening characteristics of self-taped and non-self-tapped cortical bone screws, Clin. Orthop. Rel. Res. 157 (1981) 279–286.
[14] U. Kühnapfel, H.K. Çakmak, H. Maaß, . H, Endoscopic surgery training using virtual reality and deformable tissue simulation, Comput. Graphics 24 (2000) 671–682.
[15] L. Caponetti, A.M. Fanell, Computer-aided simulation for bone surgery, IEEE Comput. Graphics Appl. 13 (1993) 87–91.
[16] P.A. Heng, C.Y. Cheng, T.T. Wong, Y. Xu, Y.P. Chui, K.M. Chan, S.K. Tso, A virtual-reality training system for knee arthroscopic surgery, IEEE Trans. Inform. Technol. Biomed. 8 (2004) 217–227.
[17] J. Xia, H.H.S. Ip, N. Samman, H.T.F. Wong, J. Gateno, D. Wang, R.W.K. Yeung, C.S.B. Kot, H. Tideman, Three-dimensional virtual-reality surgical planning and soft-tissue prediction for orthognathic surgery, IEEE Trans. Inform. Technol. Biomed. 5 (2001) 97–107.
[18] B. Pflesser, A. Petersik, U. Tiede, K.H. Höhne, R. Leuwer, Volume cutting for virtual petrous bone surgery, Comput. Aided Surg. 7 (2002) 74–83.
[19] M.D. Tsai, M.S. Hsieh, Volume manipulations for simulating bone and joint surgery, IEEE Trans. Inform. Technol. Biomed. 9 (2005) 139–149.
[20] M.D. Tsai, S.B. Jou, M.S. Hsieh, A new method for lumbar herniated inter-vertebral disc diagnosis based on image analysis of transverse sections, Comput. Med. Imag. Graph. 26 (2002) 369–380.
[21] M.S. Hsieh, M.D. Tsai, Y.D. Yeh, S.B. Jou, Automatic spinal fracture diagnosis and surgical management based on 3D image analysis and reconstruction of CT transverse sections, Biomed. Eng. Appl. Basis Commun. 14 (2002) 204–214.
[22] M.D. Tsai, Tsai, Y.D. Yeh, M.S. Hsieh, C.H. Tsai, Automatic spinal disease diagnoses assisted by 3D unaligned transverse CT slices, Comput. Med. Imag. Graph. 28 (2004) 307–319.
[23] M.D. Tsai, M.S. Hsieh, S.B. Jou, Virtual reality orthopedic surgery simulator, Comput. Biol. Med. 31 (5) (2001) 333–351.
[24] M.D. Tsai, S.B. Jou, M.S. Hsieh, Three-dimensional geometric constraint evaluation and analysis for determining commercial knee prosthesis, J. Med. Biol. Eng. 22 (2002) 139–214.
[25] M.S. Hsieh, M.D. Tsai, Y.D. Yeh, Three-dimensional hip morphology analysis using CT transverse sections to automate diagnoses and surgery managements, Comput. Biol. Med. 35 (2005) 347–371.
[26] M.S. Hsieh, M.D. Tsai, W.C. Chung, Virtual reality simulator for osteotomy and fusion involving the musculoskeletal system, Comput. Med. Imag. Graph. 26 (2002) 91–101.
[27] M.D. Tsai, W.C. Chang, M.S. Hsieh, Three-dimensional landmarking based maxillomandibular deformity diagnosis using three-dimensional computer tomography, J. Med. Biol. Eng. 22 (2002) 129–138.
[28] C. Monserrat, U. Meier, M. Alcañiz, F. Chinesta, M.C. Juan, A new approach for the real-time simulation of tissue deformations in surgery simulation, Comput. Methods Programs Biomed. 64 (2001) 77–85.
[29] U. Kühnapfel, H.K. Çakmak, H. Maaß, Endoscopic surgery training using virtual reality and deformable tissue simulation, Comput. Graphics 24 (2000) 671–682.
[30] K.S. Choi, H. Sun, P.A. Hen, Interactive deformation of soft tissues with haptic feedback for medical learning, IEEE Trans. Inform. Technol. Biomed. 7 (2003) 358–363.
[31] T.Y. Lee, C.H. Lin, H.Y. Lin, Realistic rendering of an organ surface in real-time for laparoscopic surgery simulation, Visual Comput. 18 (2002) 135–149.
[32] S. Cotin, H. Delingette, N. Ayache, A hybrid elastic model for real-time cutting, deformations, and force feedback for surgery training and simulation, Visual Comput. 16 (2000) 437–452.
[33] M. Agus, A. Giachetti, E. Gobbetti, G. Zanetti, A. Zorcolo, Adaptive techniques for real-time haptic and visual simulation of one dissection, in: Proceedings of the IEEE Virtual Reality, 2003, pp. 102–109.
[34] G. Thomas, L. Johnson, S. Dow, C. Stanford, The design and testing of a force feedback dental simulator, Comput. Methods Programs Biomed. 64 (2001) 53–64.
[35] M.S. Hsieh, M.D. Tsai, Y.D. Yeh, An amputation simulator with bone sawing haptic interaction, Biomed. Eng. Appl. Basis Commun. 18 (2006) 229–236.
[36] J.S. Strenkowski, C.C. Hsieh, A.J. Shih, An analytical finite element technique for predicting thrust force and torque in drilling, Int. J. Mach. Tools Manuf. 44 (2004) 1413–1421.
[37] J.A. Yang, V. Jaganathan, R. Du, A new dynamic model for drilling and reaming processes, Int. J. Mach. Tools Manuf. 42 (2002) 299–311.
[38] A. Langella, L. Nele, A. Maio, A torque and thrust prediction model for drilling of composite materials, Composites Part A 36 (2005) 83–93.
[39] S. Ema, E. Marui, Theoretical analysis on chatter vibration in drilling and its suppression, Mater. Process. Technol. 138 (2003) 572–583.
[40] T.M. Massie, J.K. Salisbury, The PHANToM haptic interface: a device for probing virtual objects, in: Proceedings of the ASME Haptic Interfaces for Virtual Environment and Teleoperator Systems in Dynamic Systems and Control, vol. 1, 1994, pp. 295–301.
[41] R.S. Aliva, L.M. Sobicrajski, A haptic interaction for volume visualization, in: Proceedings of the IEEE Visualization, 1996, pp. 197–204.
[42] J.E. Colgate, M.C. Stanley, J.M. Brown, Issues in the haptic display of tool use, in: Proceedings of the IEEE Intelligent Robots and Systems: Robot Interaction and Cooperative Robots, 1995, pp. 140–145.

Ming-Dar Tsai received his B.S. degree in mechanical engineering from National Taiwan University, Taipei, Taiwan, in 1983, and M.S. and Ph.D. degrees in precision machinery engineering from the University of Tokyo, Japan, in 1988 and 1991, respectively. Since 1991, he has been a member of the faculty of the Department of Information and Computer Engineering of Chung Yuan Christian University, Chungli, Taiwan, where he is currently a professor. His research interests include computer graphics, virtual reality, and scientific visualization and computer applications in medicine.

Ming-Shium Hsieh received his M.D. degree from Taipei Medical University, Taiwan, in 1974, and a Ph.D. degree in Orthopedic Surgery from Essen University, Germany, in 1982. Since 1986, he has been on the faculty of the Department of Orthopedics at Taipei Medical University, Taipei, Taiwan, where he is currently the chairman and a professor. His research interests include image studies, computer graphics, virtual reality, computer application in medicine and orthopedics including spinal surgery, arthroplasty, traumatology and basic research of orthopedics.

Chiung-Hsin Tsai received his B.S. degree in power mechanical engineering from National Tsing Hua University, Hsinchu, Taiwan, in 1980, and M.S. degrees in machinery engineering from the National Sun Yat-sen University, Kaohsiung, Taiwan, in 1985, respectively. Since 1988, he has been an assistant professor at the Lunghwa University of Science and Technology, Taoyun, Taiwan. His research interests include microprocessor system application, automatic control and image processing.